Journal of Power Sources 212 (2012) 100–104

Contents lists available at SciVerse ScienceDirect

Journal of Power Sources

journal homepage: www.elsevier.com/locate/jpowsour

Mimetic underpotential deposition technique extended for surface nanoengineering of electrocatalysts

Shao-Hua Wang, Han-Xuan Zhang, Wen-Bin Cai*

Shanghai Key Laboratory for Molecular Catalysis and Innovative Materials, and Department of Chemistry, Fudan University, Shanghai 200433, China

ARTICLE INFO

Article history:
Received 17 January 2012
Received in revised form
15 March 2012
Accepted 17 March 2012
Available online 10 April 2012

Keywords:
Mimetic underpotential deposition
Surface modification
Galvanic redox replacement
Electrocatalyst
Formic acid oxidation

ABSTRACT

The mimetic underpotential deposition (MUPD) technique without external potential control has been newly extended for surface decorations of Pb sub-monolayer on Pt (denoted as Pt@Pb), Pt (sub)monolayer on Au (denoted as Au@Pt), and Pt–Pd mixed monolayer on Pd (denoted as Pd@Pt–Pd), respectively, by introducing appropriate reducing agents in decorating baths. The carbon black-supported Pt@Pb catalyst (denoted as Pt@Pb/C) is obtained simply through the Pb MUPD on Pt/C whereas the Au@Pt and the Pd@Pd–Pt/C catalysts are obtained through the Cu MUPD followed a subsequent galvanic redox replacement. The electro-oxidation of formic acid is used as a model reaction to verify the effectiveness of such surface modifications. The tremendously enhanced activities on various electrocatalysts demonstrate that the extended MUPD approach is promising for scale-up skin modification on nanocatalysts with foreign adatoms.

1. Introduction

The pursuit of low temperature fuel cells as promising clean energy sources calls for ongoing improvements on the relevant catalysts by taking advantage of nanomaterial design and preparation [1–3]. A great deal of effort has been devoted to increasing their catalytic activities and reducing noble and rare metal loadings by means of alloying or texturing nanostructures with other metals [4–8]. Among them, the skin modification approach has been proved very effective because of its unique feature of conferring catalysts with enhanced activity and high utilization of precious metals [9]. A widely used approach that enables the deposition of foreign metal atoms (adatoms) on various substrates is the so-called underpotential deposition (UPD), i.e., electrodeposition at a potential more positive than the corresponding reversible Nernst potential, allowing the control of the deposits at (sub)monolayer level [10–12].

Over the past decades, UPDs of IIIA, IVA and VA group metals on Pt electrodes [13,14], Cu on Au [15–17], Pt [18,19] and Pd [20,21], and Pt [22–24], Rh and Sn on Pt [25], have been reported and tested for the electrocatalytic oxidations of formic acid (FA) [13,15,16,24] and methanol [20,25,26] as well as the reduction of oxygen [18–21,26]. Notably, Adzic's group proposed a tactic combining Cu UPD and galvanic redox replacement [27] for the controlled decoration of Pt adatoms on metal surfaces, further expanding the application of the Cu UPD [19,20]. Recently, Wang et al. reported NPG–Pt_1–Au_x electrocatalyst based on combined Cu UPD–redox replacement on nanoporous Au (NPG) sheet, leading to a significantly enhanced performance for FA oxidation [16]. However, all the above-mentioned UPD-involved surface modifications require external electricity controls, and thus their applicability is limited to regular bulk electrodes or nanocatalysts-coated electrodes, and may not be suited for scale-up surface modification on powder nanocatalysts as-synthesized or commercially supplied.

To address this issue, we proposed an electroless mimetic underpotential deposition (MUPD) which exploits suitable reductants to adjust the open circuit potential (OCP) of a metallic substrate in a decorating bath to a suitable UPD potential [28]. Later, Adzic's group [21] reported a specially designed electrochemical cell with its conducting inner wall as the working electrode and the Pd/C catalyst powder suspended in electrolyte was mechanically stirred to continually hit the inner wall of the cell to attain the electrochemical Cu UPD on Pd surfaces. Since our MUPD is an all-wet chemical immersion process without any external potential control, it is expected to benefit scale-up surface modification for various types of catalysts, including but not limited to the powder form. Nevertheless, initial success of this MUPD approach was only exemplified with the case of decorating Sb on Pt surfaces [28], and

* Corresponding author. Tel./fax: +86 21 55664050.
E-mail address: wbcai@fudan.edu.cn (W.-B. Cai).

0378-7753/$ – see front matter © 2012 Elsevier B.V. All rights reserved.
doi:10.1016/j.jpowsour.2012.03.060

further development of this method is thus highly demanded for its wider applications.

In this work, we aim to extend the MUPD strategy to the decoration of Pb on Pt surfaces, and Cu on *M* surfaces (*M* = Pt, Pd and Au) by introducing appropriate reducing agents. In conjunction with subsequent galvanic redox replacement, the surface Cu atoms can further be replaced with Pt or mixed Pt and Pd adatoms. The electro-oxidation of FA which is relevant to the anode reaction in a direct formic acid fuel cell (DFAFC) was chosen as a model reaction to examine the effectiveness of this approach for modifying the metallic surfaces in both bulk and powder forms. The results open a promising avenue to impart sizably existing carbon supported or unsupported Pt and Pd nanocatalysts with higher electrocatalytic activities towards (but not limited to) FA oxidation.

2. Experimental

2.1. Surface modification

All chemicals used in the preparation procedure were of analytical reagent grade and purchased from Sinophram Chemical Reagent Co., Ltd. Milli-Q water (≥18.2 MΩ cm, Millipore) was used throughout the experiments.

The procedure for Pb MUPD on Pt surfaces or Cu MUPD on Au surfaces was similar to that described in our previous work [28] and shown in Scheme 1. For surface decoration of Pb adatoms on a Pt disk (Φ = 2 mm), the Pt electrode was immersed in 0.1 mM $Pb(NO_3)_2$ and 2 mM ascorbic acid (AA) at 25 °C for 2 min to form Pb MUPD on Pt surfaces (denoted hereafter as Pt@Pb); For surface decoration of Cu adatoms on a Au disk (Φ = 3 mm), the Au electrode was immersed in deaerated 0.5 mM $CuSO_4$ and 5 mM glyoxal at 30 °C for 20 min to attain Cu MUPD on Au surfaces (denoted hereafter as Au@Cu). The MUPD-modified electrodes were rinsed with copious amount of ultrapure Milli-Q water for further measurement or treatment. The Au@Cu electrode was then transferred to a solution of 1 mM H_2PtCl_6 and 0.1 M H_2SO_4, and stored for 10 min to form the Au@Pt electrode via the galvanic redox replacement reaction. For the Cu MUPD–redox replacement, all solutions were deaerated beforehand with an ultrapure argon flow for 40 min to minimize possible oxidation of Cu MUPD layer by the dissolved oxygen.

Pb MUPD on powdered Pt nanoparticles was attained either on a Pt/C (20 wt.%, E-TEK) nanocatalyst-coated glassy carbon (GC) electrode or in an aqueous suspension of the Pt/C. For the former (denoted hereafter as Pt@Pb/C-MUPD-a), the commercial Pt/C catalyst was coated on a GC rotating disk electrode (GC-RDE) in a same protocol as-described in subsection 2.3, and then the electrode was soaked in a bath containing 0.1 mM $Pb(NO_3)_2$ and 2 mM AA at 25 °C for 20 min. A longer immersion time than that for the bulk Pt electrode was needed to achieve a given Pb coverage on Pt nanoparticles trapped in the Pt/C-Nafion mixed overlayer. For the latter (denoted hereafter as Pt@Pb/C-MUPD-b), the Pt/C powder was suspended in Milli-Q water under sonication for 1 h and then transferred into a solution containing 0.1 mM $Pb(NO_3)_2$ and 2 mM AA at 25 °C for ca. 2 min, followed by a fast filtration and a thorough rinse with Milli-Q water. The Pt@Pb/C powder thus obtained was dried at 50 °C under vacuum. In contrast, irreversible adsorption (IRA) of Pb on Pt surfaces of supported Pt/C overlayer and dispersed Pt/C in neat 0.1 mM $Pb(NO_3)_2$ leads to the samples denoted respectively as Pt@Pb/C-IRA-a and Pt@Pb/C-IRA-b. For surface modification of the Pd/C nanocatalyst (40 wt.%, BASF) with MUPD of Cu and subsequent galvanic redox replacement, a similar procedure was adopted except that aliquots of ethanol (the final volume ratio of water to ethanol was 7:1) were added respectively to the MUPD solution containing 0.5 mM $CuSO_4$ and the redox replacement solution containing 0.1 mM K_2PtCl_4, 0.9 mM H_2PdCl_4 and 0.1 M H_2SO_4 to achieve a better dispersion of Pd/C nanoparticles. After being sonicated, and separated by centrifugation, the mixed Pd and Pt adatoms-decorated Pd/C (denoted hereafter as Pd@Pd–Pt/C) catalyst was dried at 70 °C under vacuum.

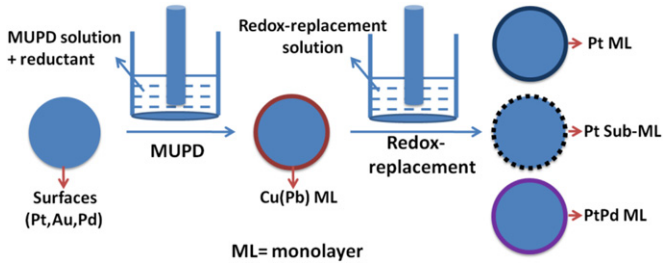

Scheme 1. Schematic diagram for MUPD–redox replacement procedure.

2.2. Materials characterizations

The chemical composition of the as-prepared catalysts was evaluated with inductively coupled plasma-atomic emission spectroscopy (ICP-AES, Hitachi P-4010) by determining the concentration of dissolved metallic species from the catalyst powder using hot aqua regia of a known volume. The morphology of the nanoparticles was examined by transmission electron microscopy (TEM) with a JEM-2100F microscope.

2.3. Electrochemical measurements

Electrochemical measurements were run on a CHI660B workstation (CH Instruments, Shanghai) in deaerated 0.5 M H_2SO_4, or 0.5 M H_2SO_4 and 0.5 M HCOOH (FA). Either the above-mentioned Au and Pt disks or the nanocatalyst-coated GC-RDEs served as the working electrodes. A Pt sheet was used as the counter electrode, a saturated mercurous sulphate electrode as the reference electrode to avoid the interference of Cl^-. However, all the following potentials were quoted with respected to saturated calomel electrode (SCE). All electrochemical measurements were performed at 30 °C.

The catalyst ink was prepared by dispersing 1 mg of the as-prepared Pt@Pb/C or Pd@Pd–Pt/C in a solution containing 750 μL of ultrapure water and 170 μL of absolute ethanol mixed with 80 μL of Nafion (5 wt.% ethanol solution, Aldrich) under sonication for 30 min. Then, a desired amount of the ink was spread on a GC-RDE (Φ = 5 mm) via a transfer pipette to attain a Pd loading of 28 μg cm^{-2} and then was naturally dried at room temperature. A similar procedure was used to prepare a Pt@Pb/C-coated GC electrode, with a Pt loading of 28 μg cm^{-2}.

3. Results and discussion

Two parallel pathways are commonly assumed for the electro-oxidation of FA at Pt electrodes, namely, (1) direct dehydrogenation pathway to form CO_2 via possibly the formate intermediate species and (2) indirect oxidation pathway which involves a dehydration step to yield water and adsorbed CO and its further oxidation to CO_2 at high potentials. CO poisoning due to the dehydration of FA on three contiguous surface Pt atoms hinders the dehydrogenation of FA at lower overpotentials [29]. Breaking the continuity of surface Pt sites can be achieved through either depositing other foreign atoms onto a Pt electrode or depositing scattered Pt adatoms on other electrodes. If so, not only the dehydration pathway is inhibited due to the so-called “third-body”

effect, but the surface electronic properties may be also modified, enhancing the dehydrogenation pathway [6]. In line with this argument, three cases of surface modifications are designed based on our extended MUPD approach and tested for their electrocatalytic activity towards FA oxidation in the following.

3.1. MUPD and MUPD-redox replacement

Different from the traditional UPD that is suited for bulk electrodes, the MUPD is generally applicable to modify either bulk or powder samples without external electricity supplies. The corresponding OCPs for Pt, Au and Pd electrodes decreased from 0.48, 0.33 and 0.35 V to 0.12, 0.27 and 0.15 V, respectively, with the addition of appropriate reductants in the precursor baths to remove surface oxide adlayers that were spontaneously preformed on the above metal substrates. These OCPs are close to the reported potentials used for Pb UPD on Pt [22], Cu UPD on Au [15], and Cu UPD on Pd [21]. The negative shift of OCPs combined with controlled immersion times enabled reasonable coverages of foreign metals on the substrates to be obtained. The redox-replacement reaction time (10 min) was chosen to ensure the Cu MUPD layer to be replaced by a more noble metal to a largest extent.

3.2. Case study

3.2.1. Pt@Pb bulk electrode & Pt@Pb/C

Fig. 1A compares cyclic voltammograms (CVs) within hydrogen adsorption/desorption potential region in 0.5 M H_2SO_4 for Pt and Pt@Pb bulk electrodes prepared by MUPD method and IRA method. The decreased hydrogen adsorption–desorption charge indicates that Pb adatoms were decorated on Pt electrode surfaces. The θ_{Pb} of ca. 0.3 was calculated based on the difference of hydrogen adsorption–desorption charges with/without the Pb adlayer, which is close to the optimal θ_{Pb} value (ca. 0.35 [13]) for FA oxidation. In contrast, Pb IRA on Pt electrode in $Pb(NO_3)_2$ solution in the absence of AA leads to a much lower θ_{Pb} value, and thus a less enhanced oxidation activity.

Furthermore, two specific measures of the MUPD method were applied to the Pb skin modification on a Pt/C catalyst and FA oxidation reaction was used to demonstrate the versatility. Fig. 1B shows CVs within the hydrogen adsorption/desorption potential region for the Pt@Pb/C-MUPD, Pt@Pb/C-IRA and Pt/C-coated GC electrodes, similar to those observed in Fig. 1A in terms of a higher Pb coverage with AA in the Pb-decorating bath. Fig. 1C shows the forward-scan voltammograms for Pt@Pb/C-MUPD-a, Pt@Pb/C-IRA-a, and Pt/C-coated GC-RDEs in 0.5 M H_2SO_4 + 0.5 M FA at 50 mV s^{-1} and 1000 rpm, with the inset corresponding to those for Pt@Pb/C-MUPD-b, Pt@Pb/C-IRA-b. The voltammetric profile for the Pt/C is characterized by a very low anodic peak at ca. 0.68 V with a shoulder at ca. 0.3 V, indicating that the electro-oxidation of FA on an unmodified Pt/C is greatly hindered by strongly adsorbed CO due to the dehydration of FA. In contrast, on Pb-modified Pt electrodes, the FA oxidation currents were significantly enhanced with a broad peak locating at ca. 0.3 V and a shoulder at ca. 0.68 V. The enhanced dehydrogenation may be ascribed to the so-called "third-body effect" as well as the electronic effect owing to discrete Pb adatoms on Pt surfaces [30].

The durability of catalysts was considered as another important issue for scale-up applications. Along this line, the long-term performances of these catalysts were further examined by chronoamperometric measurements, conducted on catalyst-coated GC-RDEs at 1000 rpm in 0.5 M H_2SO_4 + 0.5 M FA with the potential stepped from OCP (ca. −0.2 V) to 0.25 V, as shown in Fig. 1D. The initial current density decreased in the order of Pt@Pb/C-

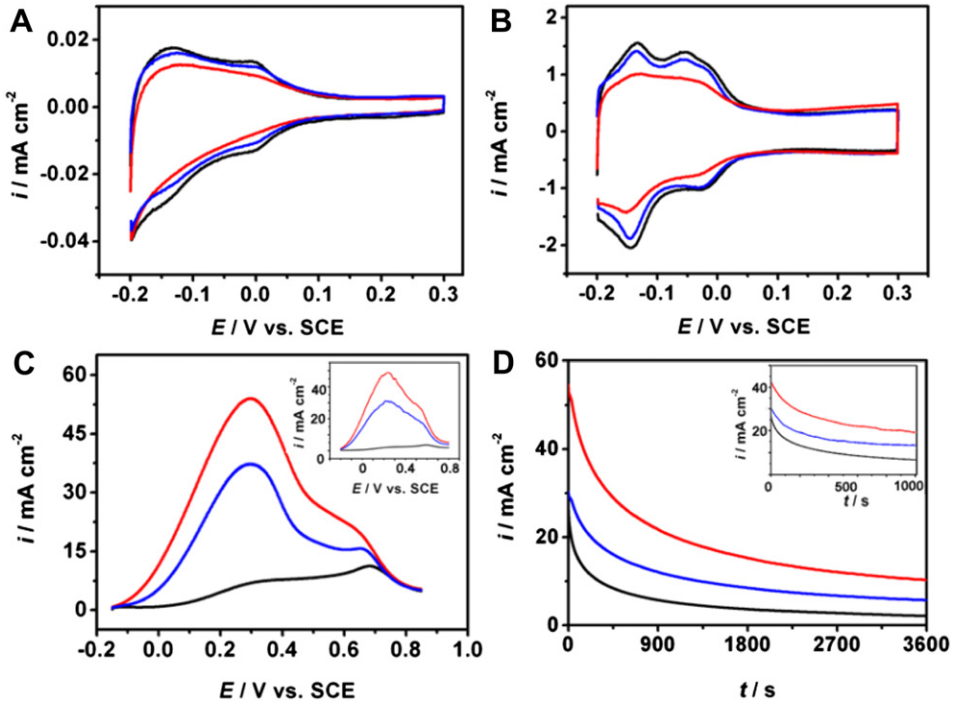

Fig. 1. CVs in the hydrogen adsorption/desorption potential region in 0.5 M H_2SO_4 at 50 mV s^{-1} for (A) Pt@Pb-MUPD, Pt@Pb-IRA and Pt electrodes, and (B) Pt@Pb/C-MUPD-a, Pt@Pb/C-IRA-a and Pt/C-coated GC RDEs. (C) CVs for Pt@Pb/C-MUPD-a, Pt@Pb/C-IRA-a, and Pt/C-coated GC-RDEs in 0.5 M FA and 0.5 M H_2SO_4 at 50 mV s^{-1} and ω = 1000 rpm. The inset shows CVs for Pt@Pb/C-MUPD-b, Pt@Pb/C-IRA-b, and Pt/C-coated GC-RDEs under otherwise same conditions. (D) i–t curves measured for Pt@Pb/C-MUPD-a, Pt@Pb/C-IRA-a, and Pt/C-coated GC-RDEs at 0.25 V vs. SCE in 0.5 M FA and 0.5 M H_2SO_4, ω = 1000 rpm. The inset is i–t curves for Pt@Pb/C-MUPD-b, Pt@Pb/C-IRA-b, and Pt/C catalyst-coated GC-RDEs under otherwise same conditions. Red, blue and black curves in the above plots correspond to Pb MUPD, Pb-IRA decorated and undecorated Pt surfaces, respectively. (For interpretation of the references to colour in this figure legend, the reader is referred to the web version of this article.)

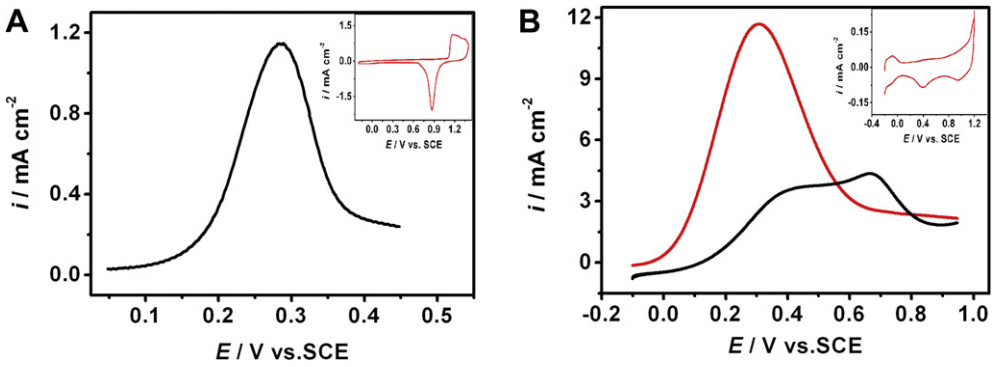

Fig. 2. (A) The anodic stripping voltammogram for the Au@Cu electrode in 0.5 M H_2SO_4, at a scan rate of 400 mV s^{-1}. The inset is the CV on the unmodified Au electrode in 0.5 M H_2SO_4, at a scan rate of 400 mV s^{-1}. (B) CVs for FA oxidation on the Au@Pt electrode (red line) and Pt film electroplated on Au electrode (black line) in 0.5 M FA and 0.5 M H_2SO_4, at 50 mV s^{-1} and $\omega = 1000$ rpm. The inset is the CV for the above Au@Pt electrode in 0.5 M H_2SO_4, at a scan rate of 100 mV s^{-1}. (For interpretation of the references to colour in this figure legend, the reader is referred to the web version of this article.)

MUPD > Pt@Pb/C-IRA > Pt/C, consistent with the results in Fig. 1C. On the other hand, the Pt@Pb/C-MUPD also exhibits the best catalytic activity as compared to its counterparts throughout the *i*–*t* test, suggesting a good electrochemical durability for the catalysts as modified by the MUPD method.

3.2.2. Au@Pt

The Cu MUPD on Au (denoted hereafter as Au@Cu) electrode was swept at 400 mV s^{-1} from −0.25 V to 0.5 V to strip the Cu adlayer from Au (Fig. 2A). The stripping peak around 0.3 V for the MUPD Cu is similar to that for a regular UPD Cu on Au electrode [31]. A typical CV for a bulk Au electrode is shown in the inset of Fig. 2A from which the reduction charge for Au oxide monolayer contained in the reduction peak at 0.89 V can be obtained.

The amount of MUPD Cu, n_{Cu}, can be estimated from its anodic stripping charge (Q) :

$$Q = S/\nu,\ n_{Cu} = Q/nF$$

where S is the integral area of the stripping peak, ν is the scan rate, F is the Faraday constant and n equals to 2. By comparing the Cu stripping charge (2.6×10^{-5} C) with the Au oxide reduction charge (4.8×10^{-5} C), a Cu coverage of ca. 54% can be estimated. Through the subsequent redox-replacement reaction in the $PtCl_6^{2-}$-containing solution, the Au@Pt electrode was obtained with the deposited Pt amount of ca. 6.6×10^{-11} mol, given a 100% replacement of Cu ($n_{Cu} = 1.32 \times 10^{-10}$ mol) by Pt. In fact, the MUPD Cu atoms cannot be replaced completely by using this process. According to our ICP-AES analysis, 11–16% of the MUPD Cu remained on an Au or Pd substrate, consistent with 13% of UPD Cu intact on Au/C in a previous report regarding the surface-limited galvanic replacement with Pt [17].

Notably, the MUPD did not yield a monolayer coverage of Cu on the Au surface, and with the galvanic redox replacement in a Pt (IV)-solution, the Pt on the Au surface corresponds to coverage of

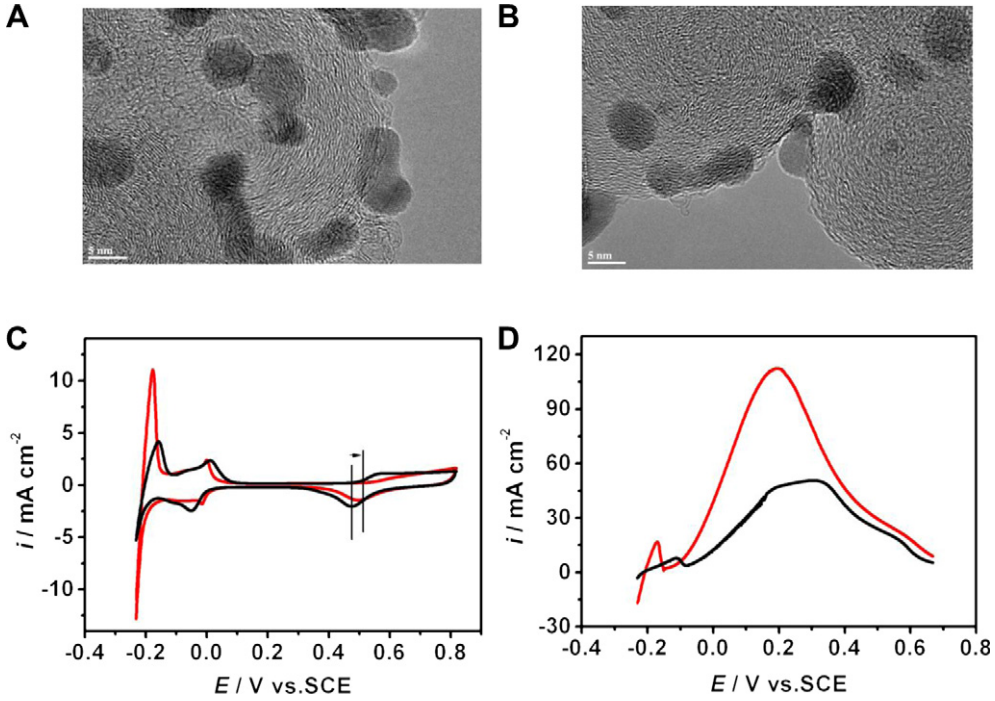

Fig. 3. TEM images of the Pd@Pd–Pt/C (A) and Pd/C (BASF) (B). CVs for the Pd@Pd–Pt/C (red line) and the Pd/C (black line)-coated GC-RDEs in 0.5 M H_2SO_4 at 50 mV s^{-1} (C). Positive-going voltammograms for Pd@Pd–Pt/C (red line) and Pd/C (black line)-coated GC-RDEs in 0.5 M FA and 0.5 M H_2SO_4 at 50 mV s^{-1} and $\omega = 1000$ rpm (D). (For interpretation of the references to colour in this figure legend, the reader is referred to the web version of this article.)

ca. 0.25. Nevertheless, this low coverage benefits the discontinuity of surface Pt atoms on Au substrate, inhibiting the dehydration pathway to form the CO poisoning species on Pt sites. The inset of Fig. 2B shows the CV for the Au@Pt electrode in blank 0.5 M H_2SO_4. The hydrogen adsorption/desorption peaks at potentials negative of 0.1 V SCE is characteristic of the decorated Pt adlayer on Au electrode, in addition to the cathodic peaks for exposed surface Au oxide (at ca. 1.0 V) and Pt oxide (at ca. 0.4 V).

Fig. 2B shows the positive-going voltammograms for the Au@Pt electrode and an electroplated thick Pt film on Au electrode in 0.5 M FA and 0.5 M H_2SO_4 at 50 mV s^{-1} at 1000 rpm. Interestingly, the Au electrode surface modified with very small amount of Pt can dramatically enhance the FA oxidation activity at rather low oxidation potentials, as compared to the thick Pt film electrode. To quantify the specific activity of Pt atoms towards FA oxidation, the measured peak current at 0.3 V is also normalized by the total number of Pt atoms (the bare Au has a negligible contribution to the oxidation current), leading to a specific activity of 3.3×10^{-17} A per Pt atom, which is 10 times more active for FA oxidation than the counterpart reported in literature [15].

3.2.3. Pd@Pd–Pt/C

ICP-AES analysis on the prepared Pd@Pd–Pt/C indicated the loading of decorated Pt atoms accounts for ca. 0.9 wt% of the carbon-supported catalyst, and about 15% of the MUPD Cu yet remained unreplaced. The TEM image of the Pd@Pd–Pt/C catalyst is shown in Fig. 3A, together with that of the unmodified Pd/C in Fig. 3B. The Pd@Pd–Pt nanoparticles are well dispersed on carbon black and their mean size is largely close to that of the Pd/C sample. This observation is in agreement with the nature of surface-limited galvanic replacement reaction in which a sub-monolayer of mixed Pt and Pd adatoms is expected to decorate on underlying Pd nanoparticle cores.

Fig. 3C shows the CVs for the Pd@Pd–Pt/C and the Pd/C-coated GC-RDEs in 0.5 M H_2SO_4 at a scan rate of 50 mV s^{-1} at 1000 rpm. With the surface decoration of mixed Pt and Pd atoms, the hydrogen adsorption (absorption) and oxidative desorption peaks change significantly together with the oxide formation and reduction features. Specifically the facile hydrogen oxidation and oxide reduction linked to the Pd@Pd–Pt/C resembles our previous results obtained with Pd_xPt_{1-x} alloys of low Pt contents [6]. The above electrochemical features can't be explained by the simple coaddition of two separated contributions of surface Pd and Pt domains, rather it may be better considered as a result of their coeffect, which may involve inhibited dehydration of FA on Pt sites and a slightly decreased d-band centre on Pd sites [6].

The as-formed Pd@Pd–Pt/C was used as the catalyst for FA oxidation by coating it on a GC-RDE which was then tested in 0.5 M H_2SO_4 and 0.5 M FA with cyclic voltammetry. Shown in Fig. 3D is the positive-going voltammogram from −0.2 V, the peak current density for FA oxidation on the Pd@Pd–Pt/C is 112 mA cm^{-2}, nearly twice as that on Pd/C (BASF) catalysts. Also notable is that both onset and peak potentials shift negatively for the Pd@Pd–Pt/C as compared to that for the Pd/C. In other words, the Pd@Pd–Pt/C thus formed did exhibit greatly enhanced electrocatalytic activity for the FA oxidation reaction. Further optimization of surface modification conditions is under way in order to achieve desired nanocatalysts with practically acceptable activity and durability.

4. Conclusions

An electroless UPD method, i.e., MUPD has been extended to the decoration of Pb on Pt surfaces, and the decoration of Cu on Au and Pd surfaces as well. The trick is to introduce an appropriate reducing agent in a Pb(II) or Cu(II)-containing electrolyte to regulate the open circuit potential of a desired substrate down to one that can be used for conventional sub-monolayer UPD. In combination with subsequent redox replacements, the Cu decorated Au and Pd surfaces can be further changed to Pt adatoms-decorated Au and mixed Pd and Pt-adatoms-decorated Pd surfaces, respectively. The validity and versatility of the above approach is examined with the model reaction, namely formic acid oxidation. Indeed, the as-formed bulk and powder electrocatalysts Pt@Pb, Pt@Pb/C, Au@Pt and Pd@Pd–Pt/C all exhibit greatly enhanced electrocatalytic activity towards FA oxidation, as compared to unmodified surfaces or surfaces modified using conventional irreversible adsorption. Since all the processes involved are wet chemical ones without external electrical control, this newly extended approach is particularly suitable for scale-up surface modification of Pt, Pd and Au-based electrocatalysts towards higher performances.

Acknowledgements

We appreciate Dr. Bin Peng for his valuable suggestions. This work is supported by NSFC (Nos. 20833005 and 21073045), SMCST (Nos. 11JC400300 and 08DZ2270500). The State Key Laboratory of ASIC & System (Fudan University) supports the purchase of chemicals.

References

[1] J. Lee, S. Uhm, H.J. Lee, Phys. Chem. Chem. Phys. 11 (2009) 9326–9336.
[2] X.W. Yu, P.G. Pickup, J. Power Sources 182 (2008) 124–132.
[3] H.S. Liu, C.J. Song, L. Zhang, J.J. Zhang, H.J. Wang, D.P. Wilkinson, J. Power Sources 155 (2006) 95–110.
[4] J. Ge, W. Xing, X. Xue, C. Liu, T. Lu, J. Liao, J. Phys. Chem. C 111 (2007) 17305–17310.
[5] J.Y. Wang, Y.Y. Kang, H. Yang, W.B. Cai, J. Phys. Chem. C 113 (2009) 8366–8372.
[6] H.X. Zhang, C. Wang, J.Y. Wang, J.J. Zhai, W.B. Cai, J. Phys. Chem. C 114 (2010) 6446–6451.
[7] Y. Jiang, J. Zhang, Y.H. Qin, D.F. Niu, X.S. Zhang, L. Niu, X.G. Zhou, T.H. Lu, W.K. Yuan, J. Power Sources 196 (2011) 9356–9360.
[8] L. Dai, S. Zou, J. Power Sources 196 (2011) 9369–9372.
[9] V.R. Stamenkovic, B.S. Mun, K.J.J. Mayrhofer, P.N. Ross, N.M. Markovic, J. Am. Chem. Soc. 128 (2006) 8813–8819.
[10] D.M. Kolb, M. Przasnys, H. Gerische, J. Electroanal. Chem. 54 (1974) 25–38.
[11] A.I. Danilov, R.R. Nazmutdinov, T.T. Zinkicheva, E.B. Molodkina, A.V. Rudnev, Y.M. Polukarov, J.M. Feliu, Russ. J. Electrochem. 44 (2008) 697–708.
[12] J.W. Yan, J. Tang, Y.Y. Yang, J.M. Wu, Z.X. Xie, S.G. Sun, B.W. Mao, Surf. Interface Anal. 32 (2001) 49–52.
[13] M. Watanabe, M. Horiuchi, S. Motoo, J. Electroanal. Chem. 250 (1988) 117–125.
[14] D.R. Wheeler, J.X. Wang, R.R. Adzic, J. Electroanal. Chem. 387 (1995) 115–119.
[15] Y.L. Yu, Y.P. Hu, X.W. Liu, W.Q. Deng, X. Wang, Electrochim. Acta 54 (2009) 3092–3097.
[16] R.Y. Wang, C. Wang, W.B. Cai, Y. Ding, Adv. Mater. 22 (2010) 1845–1849.
[17] M. Fayette, Y. Liu, D. Bertrand, J. Nutariya, N. Vasiljevic, N. Dimitrov, Langmuir 27 (2011) 5650–5658.
[18] T. Abe, G.M. Swain, K. Sashikata, K. Itaya, J. Electroanal. Chem. 382 (1995) 73–83.
[19] J. Zhang, K. Sasaki, E. Sutter, R.R. Adzic, Science 315 (2007) 220–222.
[20] R.R. Adzic, J. Zhang, K. Sasaki, M.B. Vukmirovic, M. Shao, J.X. Wang, A.U. Nilekar, M. Mavrikakis, J.A. Valerio, F. Uribe, Top. Catal. 46 (2007) 249–262.
[21] K. Sasaki, J.X. Wang, H. Naohara, N. Marinkovic, K. More, H. Inada, R.R. Adzic, Electrochim. Acta 55 (2010) 2645–2652.
[22] B.N. Grgur, N.M. Markovic, P.N. Ross, Langmuir 13 (1997) 6370–6374.
[23] C. Nishihara, K. Iwata, T. Tai, M. Yuasa, I. Sekine, H. Nozoye, Electrochem. Commun. 1 (1999) 104–107.
[24] S.Y. Uhm, S.T. Chung, J.Y. Lee, Electrochem. Commun. 9 (2007) 2027–2031.
[25] Z.D. Wei, L.L. Li, Y.H. Luo, C. Yan, C.X. Sun, G.Z. Yin, P.K. Shen, J. Phys. Chem. B 110 (2006) 26055–26061.
[26] M. Khosravi, M.K. Amini, Int. J. Hydrogen Energy 35 (2010) 10527–10538.
[27] S.R. Brankovic, J.X. Wang, R.R. Adzic, Surf. Sci. 474 (2001) L173–L179.
[28] B. Peng, J.Y. Wang, H.X. Zhang, Y.H. Lin, W.B. Cai, Electrochem. Commun. 11 (2009) 831–833.
[29] A. Cuesta, M. Escudero, B. Lanova, H. Baltruschat, Langmuir 25 (2009) 6500–6507.
[30] M. Neurock, M. Janik, A. Wieckowski, Faraday Discuss. 140 (2008) 363–378.
[31] M.A. Schneeweiss, D.M. Kolb, Phys. Status Solid A 173 (1999) 51–71.